


## Comparative analysis of reconstructed architectures from mice and human islets

Gerardo J. Félix-Martínez <sup>a,b</sup> and J. R. Godínez-Fernández<sup>b</sup>

<sup>a</sup>Cátedras CONACYT, Consejo Nacional de Ciencia y Tecnología, México City, México; <sup>b</sup>Department of Electrical Engineering, Universidad Autónoma Metropolitana, México City, México

### ABSTRACT

Intra-islet communication via electrical, paracrine and autocrine signals, is highly dependent on the organization of cells within the islets and is key for an adequate response to changes in blood glucose and other stimuli. In spite of the fact that relevant structural differences between mouse and human islet architectures have been described, the functional implications of these differences remain only partially understood. In this work, aiming to contribute to a better understanding of the relationship between structural and functional properties of pancreatic islets, we reconstructed human and mice islets in order to perform a structural comparison based on both morphologic and network-derived metrics. According to our results, human islets constitute a more efficient network from a connectivity viewpoint, mainly due to the higher proportion of heterotypic contacts between islet cells in comparison to mice islets.

### ARTICLE HISTORY

Received 11 July 2021  
Revised 24 September 2021  
Accepted 27 September 2021

### KEYWORDS

Pancreatic islets; reconstruction; network; cell-to-cell contact; architecture

### Introduction

The optimal function of pancreatic islets relies on several processes at different levels of organization: from the mechanisms at the single cell level involved in the secretion of insulin, glucagon and somatostatin from  $\beta$ ,  $\alpha$  and  $\delta$  cells, respectively, to intra-islet communication signals that, in conjunction with external regulation signals (i.e. endocrine, nutritional, neural, etc.), shape the release of islet hormones, key for the control of blood glucose homeostasis.<sup>1</sup> Specifically, within the islets,  $\alpha$ ,  $\beta$  and  $\delta$  cells regulate each other via direct electrical communication (between  $\beta$  cells<sup>2–5</sup> and  $\beta$  and  $\delta$  cells<sup>6,7</sup>), as well as paracrine and autocrine signals,<sup>8–11</sup> which are highly dependent on the composition and organization of islet cells (i.e. architecture).<sup>12–14</sup> Given the fact that islet architecture is altered in type 2 diabetes,<sup>15–18</sup> it is highly likely that intra-islet communication is consequently disturbed as a result of the disease.

Multiple studies have demonstrated that mouse and human islets differ in the composition and organization of  $\alpha$ ,  $\beta$  and  $\delta$  cells. For instance, it has been shown that mice islets have more  $\beta$  cells than human islets<sup>14,19–22</sup> (~75 vs 60%, respectively), and that human islets contain a higher proportion of  $\alpha$  and  $\delta$  cells (~30 and 10%, respectively), in

comparison with mice islets (~20 and 5%, respectively).<sup>14,19–21,23,24</sup> In addition, functional interspecies differences have also been described, mainly related to  $\beta$  cells, such as the different electrical behavior observed experimentally,<sup>25,26</sup> the glucose threshold for the secretion of insulin,<sup>27,28</sup> and the ionic channels expressed.<sup>25,26,29,30</sup>

In spite of these advances, linking the structural and functional properties of pancreatic islets has not been an easy task, as several complex mechanisms are involved at different levels of organization. Moreover, the possibility that rodent and human islets are structurally and functionally different, limits the extrapolation of experimental observations between species.

Recently, a methodology based on computational optimization was proposed to reconstruct islet architectures from experimental data,<sup>31</sup> giving as a result islets composed of non-overlapping cells, also allowing to quantify cell-to-cell contacts within the islets. Based on this methodology, in this article we reconstruct architectures of both mouse and human islets in order to perform a structural comparison between species based on common structural characteristics such as cell-to-cell contacts and islet volumes, but also on connectivity related

**CONTACT** Gerardo J. Félix-Martínez Universidad Autónoma Metropolitana  [gjfelix2005@gmail.com](mailto:gjfelix2005@gmail.com) [gjfelix@conacyt.mx](mailto:gjfelix@conacyt.mx) [gjfelix@xanum.uam.mx](mailto:gjfelix@xanum.uam.mx)  Unidad Iztapalapa. San Rafael Atlixco 186, Col. Vicentina 09340, México City, México

© 2021 The Author(s). Published with license by Taylor & Francis Group, LLC.

This is an Open Access article distributed under the terms of the Creative Commons Attribution-NonCommercial-NoDerivatives License (<http://creativecommons.org/licenses/by-nc-nd/4.0/>), which permits non-commercial re-use, distribution, and reproduction in any medium, provided the original work is properly cited, and is not altered, transformed, or built upon in any way.

metrics derived from the analysis of reconstructed architectures using a network-based approach. In addition, we evaluate the impact of  $\beta$ -cell loss in the islet connectivity and network properties.

## Material and methods

### Reconstruction of islet architectures

Human and mouse islets were reconstructed using the iterative optimization algorithm described in detail in a previous work.<sup>31</sup> In short, the reconstruction algorithm consists of proposing an initial islet using the experimental nuclei coordinates as center coordinates of spherical cells with radii assigned randomly from reported experimental distributions. At each step of the iterative optimization algorithm, a cell is randomly selected and new center coordinates and radius are proposed for the selected cell. At each iteration the number of overlapped cells is calculated and compared to the minimum value obtained during the whole process. If the number of overlapped cells calculated is lower, the change in the cell radius and center coordinates is accepted; otherwise, it could be either accepted or rejected based on a monotonically decreasing probability as a way of preventing the algorithm from reaching a

local minimum. This process is repeated until either convergence or a stop criterium is reached.

The reconstructed islets were provided in previous works by Hoang et al.<sup>22,32</sup> (available under the terms of the Creative Commons Attribution License). In total, 56 mouse and human islets were reconstructed ( $n = 28$  in both cases). Given that only the position and identity of  $\alpha$  and  $\beta$  cells were reported,  $\delta$  cells were not considered for the reconstruction process. Human islets were reconstructed using the radii distributions reported by Camunas-Soler et al.<sup>33</sup> ( $\beta$ :  $6.49 \pm 1.6 \mu\text{m}$ ,  $\alpha$ :  $5.04 \pm 0.9 \mu\text{m}$ ). On the other hand, the radii distributions of mouse islet cell given by Briant et al.<sup>34</sup> were used to reconstruct the mouse islets ( $\beta$ :  $6.9 \pm 4.5 \mu\text{m}$ ,  $\alpha$ :  $5.84 \pm 3.7 \mu\text{m}$ ).

A selection of the reconstructed human and mice islets is shown in Figure 1. As described in Table 1, most of the reconstructed islets (52 of 56) included  $> 99\%$  of the cells identified experimentally, with a considerable percentage ( $\sim 41\%$ , i.e. 23 islets) even reaching 100%. Only 4 mouse islets included a slightly lower percentage of the experimentally identified cells ( $\sim 96\%$ ). These results demonstrate that the reconstruction algorithm is capable of reconstructing islets from different species in spite of the differences in cell size, composition and distribution of cells.

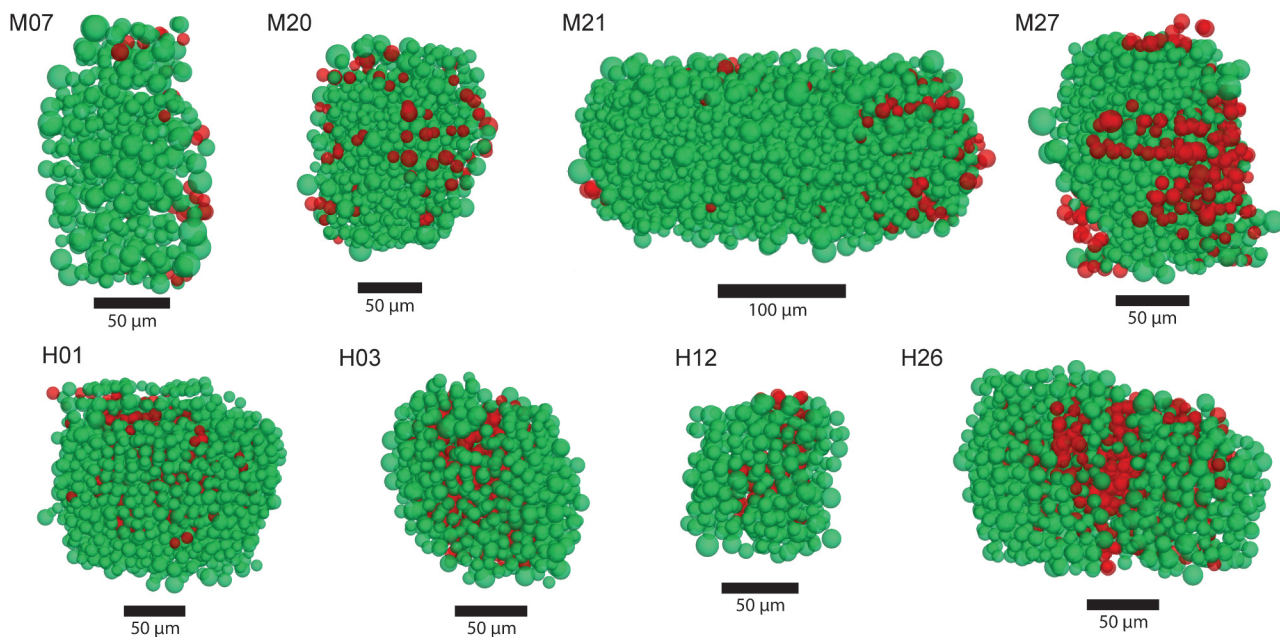


Figure 1. Selection of reconstructed human (top) and mouse (bottom) islets.

**Table 1.** Summary of the reconstruction processes

Human islets							Mice islets						
Islet	$N_{exp}$	$N_{opt}$	$N_o$	% cells	Total iterations	Computing time	Islet	$N_{exp}$	$N_{opt}$	$N_o$	% Cells	Total iterations	Computing time
1	2273	2272	1	99.96	3.28E+07	1-08:21:03	1	893	893	0	100.00	1.31E+07	0-03:43:27
2	1225	1224	1	99.92	1.63E+07	0-06:25:03	2	2598	2596	2	99.92	4.10E+07	2-09:12:59
3	1165	1160	5	99.57	1.69E+07	0-06:33:57	3	1870	1870	0	100.00	2.61E+07	0-19:20:31
4	681	681	0	100.00	8.97E+06	0-02:07:20	4	1680	1680	0	100.00	2.07E+07	0-11:43:54
5	1178	1177	1	99.92	1.39E+07	0-04:50:48	5	518	518	0	100.00	6.92E+06	0-01:31:03
6	340	340	0	100.00	4.27E+06	0-00:31:55	6	1895	1895	0	100.00	2.84E+07	0-21:44:27
7	2472	2472	0	100.00	3.34E+07	1-13:30:50	7	571	570	1	99.82	8.07E+06	0-01:47:56
8	1831	1831	0	100.00	2.67E+07	0-18:23:42	8	1192	1192	0	100.00	1.65E+07	0-06:20:00
9	916	916	0	100.00	1.22E+07	0-03:26:20	9	1153	1153	0	100.00	1.53E+07	0-05:38:56
10	2376	2374	2	99.92	3.37E+07	1-11:51:41	10	1063	1063	0	100.00	1.63E+07	0-06:23:29
11	818	818	0	100.00	1.14E+07	0-03:07:39	11	2143	2141	2	99.91	3.03E+07	1-02:47:17
12	458	457	1	99.78	7.62E+06	0-01:25:21	12	1576	1575	1	99.94	2.12E+07	0-12:12:42
13	1976	1976	0	100.00	2.97E+07	0-22:05:04	13	2471	2471	0	100.00	3.77E+07	1-22:01:13
14	536	536	0	100.00	7.04E+06	0-01:15:18	14	1113	1113	0	100.00	1.50E+07	0-05:44:00
15	1850	1849	1	99.95	2.58E+07	0-17:14:51	15	1230	1229	1	99.92	1.68E+07	0-07:13:38
16	847	842	5	99.41	1.22E+07	0-03:10:33	16	3294	3293	1	99.97	4.43E+07	4-08:18:14
17	526	526	0	100.00	6.98E+06	0-01:26:54	17	1645	1645	0	100.00	2.48E+07	0-15:29:11
18	1482	1475	7	99.53	2.19E+07	0-12:09:09	18	4159	4158	1	99.98	6.17E+07	9-09:15:32
19	1788	1785	3	99.83	2.96E+07	0-19:28:58	19	2248	2239	9	99.60	3.79E+07	1-17:37:59
20	1503	1499	4	99.73	2.28E+07	0-11:44:04	20	1182	1179	3	99.75	1.77E+07	0-08:51:03
21	1917	1916	1	99.95	2.88E+07	0-20:00:57	21	4010	4005	5	99.88	5.67E+07	8-01:15:15
22	915	914	1	99.89	1.14E+07	0-03:05:59	22	3884	3881	3	99.92	6.25E+07	8-02:14:01
23	695	694	1	99.86	1.09E+07	0-02:26:55	23	2097	2097	0	100.00	3.72E+07	1-11:38:02
24	2033	2007	26	98.72	3.36E+07	1-04:05:32	24	3209	3195	14	99.56	5.03E+07	5-04:10:10
25	613	613	0	100.00	8.61E+06	0-01:37:14	25	1631	1571	64	96.08	4.54E+07	1-07:35:39
26	1531	1530	1	99.93	2.19E+07	0-11:52:36	26	1736	1673	64	96.31	4.22E+07	1-06:48:34
27	1993	1984	9	99.55	3.05E+07	0-23:56:03	27	1430	1386	44	96.92	3.35E+07	0-20:16:03
28	2620	2620	0	100.00	4.54E+07	2-13:56:39	28	2224	2154	70	96.85	7.51E+07	3-06:30:31

$N_{exp}$ : total number of cells identified experimentally.  $N_{opt}$ : total number of cells in the reconstructed islet.  $N_o = N_{exp} - N_{opt}$ . % cells: percentage of experimental cells included in the reconstructed islets.

The computing time of the reconstruction of mouse and human islets heavily depended on the number of cells in the islet (see Table 1), ranging from ~32 minutes for an islet composed of 340 cells to more than 9 days, 9 hours and 15 minutes for a considerably larger islet (4159 cells). In terms of the number of iterations, at least  $6.92 \times 10^6$  iterations were needed to fully reconstruct an islet, while the maximum number of iterations performed were  $7.51 \times 10^7$ . Details of the reconstruction process including the computing time and number of iterations needed for all the islets reconstructed can be consulted in Table 1. Loss of  $\beta$ -cell mass was simulated by randomly removing 50% of  $\beta$ -cells from the reconstructed islets.

### Construction and analysis of islet structural networks

Undirected and unweighted networks were constructed using the cell-to-cell contacts identified during the reconstruction process, based on the assumption that cells are the network nodes and that cell-to-cell contacts are the network links. Two

different structural networks were constructed for each islet analyzed: a network composed only of  $\beta$  cells ( $\beta$ - $\beta$  network), and a network composed by both  $\alpha$  and  $\beta$  cells ( $\alpha$ - $\beta$  network). An example of the  $\beta$ - $\beta$  and  $\alpha$ - $\beta$  networks are shown in Figure 5(a). The resulting networks were therefore composed of  $N$  nodes and  $L$  links joining the nodes, with a maximum number of links given by  $L_{max} = N(N - 1)/2$ . All the networks were characterized by the following network metrics:

- (a) Average degree. Denoted by  $\langle k \rangle$ , it is the average number of links per node in the network. Given that  $k_i$  is the degree of node  $i$ , defined as the number of neighbors or links of node  $i$ , the average degree of the network was calculated as:

$$\langle k \rangle = \frac{\sum_i k_i}{N} \quad (1)$$

- (b) Density. Denoted by  $d$ , it is a measure of connectedness of the network, given by the ratio of actual cell-to-cell contacts in the network to all possible contacts

$$d = \frac{L}{L_{max}} = \frac{2L}{N(N-1)} = \frac{\langle k \rangle}{N-1} \quad (2)$$

- (c) Average clustering coefficient. Interpreted as a measure of interconnection of the neighborhood of each node in the network, it was calculated as:

$$C = \frac{\sum_{i(k_i > 1)} C_i}{N_{k_i > 1}}, \quad (3)$$

where  $C_i$  is the clustering coefficient of node  $i$ , defined as the fraction of neighbors of node  $i$  that are connected to each other. Mathematically,  $C_i$  can be calculated as:

$$C_i = \frac{\tau_i}{\tau_{max}} = \frac{2\tau_i}{k_i(k_i - 1)}, \quad (4)$$

where  $\tau_i$  and  $\tau_{max}$  are the actual number of triangles including node  $i$  and the maximum number of possible triangles that could include node  $i$ , respectively. Note that nodes with less than two neighbors (i.e.  $k_i < 2$ ) were excluded from the calculation.

- (d) Global efficiency. Defining  $d_{ij}$  as the distance between any two nodes  $i$  and  $j$  (i.e. the number of edges in the shortest path between them), the efficiency between  $i$  and  $j$  can be defined as  $e_{ij} = 1/d_{ij}$  (for  $i \neq j$ ). The global efficiency of a network is then given by the average of efficiencies over all the pairs of nodes:

$$e_g = \frac{1}{n(n-1)} \sum_{i \neq j} e_{ij} \quad (5)$$

Note that when nodes  $i$  and  $j$  are not connected,  $d_{ij} = \infty$  and  $e_{ij} = 0$ . The global efficiency can be interpreted as a measure of integration of the network.

- (e) Diameter. Given by the longest short path between all nodes in the network, it is used as a measure of size of the network.
- (f) Largest component. When a network can be described in terms of disconnected subnetworks, the largest component of the network is simply the subnetwork containing the greatest number of nodes.

## Statistical analysis

Statistical differences between human and mouse islets were assessed using the Student's t-test for the interval/ratio variables that showed a normal distribution according to the results of the Kolmogorov-Smirnov normality test and visual inspection of the data and QQ plots. Differences between species in interval/ratio variables not showing a normal distribution were assessed using the Mann-Whitney test. For comparisons of categorical variables, the  $\chi^2$  test with the Yates' correction was used. In all cases, a  $P$ -value  $< .05$  was considered to be statistically significant (\*  $P < .05$ , \*\*  $P < .01$ , \*\*\*  $P < .001$ , \*\*\*\*  $P < .0001$ ). Results are reported as mean  $\pm$  SD (standard deviation) and/or median  $\pm$  IQR (interquartile range). Throughout the article, mean and median values are denoted as  $\bar{x}$  and  $\tilde{x}$ , respectively, where  $x$  represent the variable of interest.

## Computational aspects

Islet reconstruction was performed in the Yoltla cluster of the *Laboratorio Nacional de Cómputo de Alto Desempeño* (LANCAD) at the *Universidad Autónoma Metropolitana*, Iztapalapa, México City, México. Calculations were performed in Intel Xeon E5-2670 nodes (20 physical processors and 20 threads) with 64 GB DDR3 RAM memory. Code was written in C using the OpenMP library. Postprocessing and visualization of the optimized islets were performed in Wolfram Mathematica 12.0 (Champaign, IL). Statistical analysis was performed in Prism version 9.0.0 for Mac OS (GraphPad Software, San Diego, California USA). Network analysis was performed in Python 3.7 using NetworkX.<sup>35</sup>

## Results

### Populations and volumes of $\alpha$ and $\beta$ cells in reconstructed islets

In agreement with a previous report by Hoang et al.,<sup>22</sup> mouse islets were composed of a greater number of cells than human islets (Figure 2(a)). Human islets had more  $\alpha$  cells than mouse islets, with minimum and maximum number of  $\alpha$  cells of 63 and 1162 in human islets and 19 and 469 in mouse

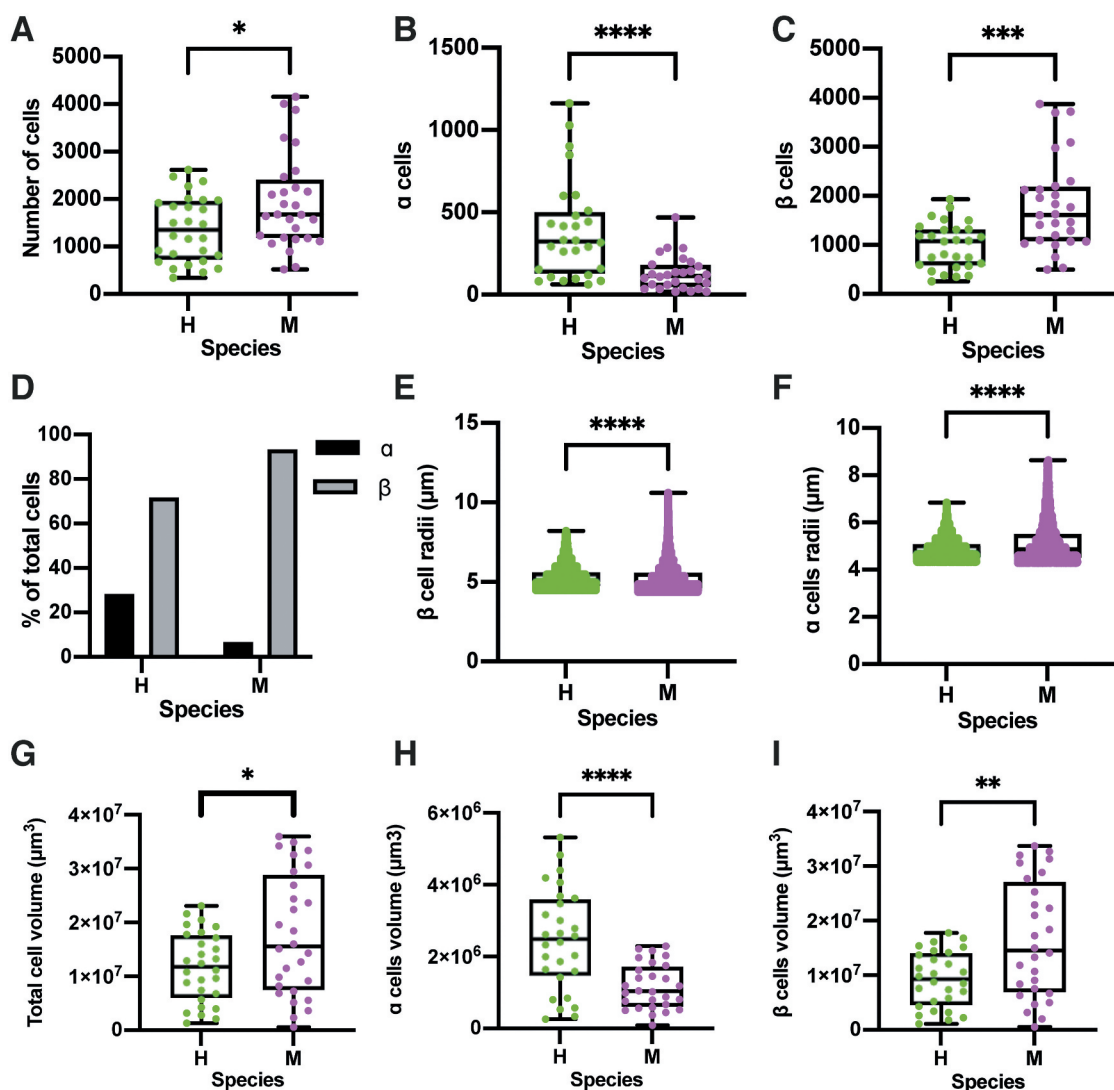


**Figure 2.** Comparison of the number of cells, cells' radii and islet volumes between human and mice islets. A. Total number of cells. B. Number of  $\alpha$  cells. C. Number of  $\beta$  cells. D. Proportion of cells. E.  $\beta$  cell radii. F.  $\alpha$  cell radii. G. Total cell volume. H.  $\beta$  cells volume. I.  $\alpha$  cells volume.

islets (Figure 2(b)). In contrast, mouse islets had more  $\beta$  cells than human islets, with the number of  $\beta$  cells ranging from 257 to 1931 in human islets and from 498 to 3876 in mouse islets (Figure 2(c)).

**Table 2.** Basic characteristics of human and mice islets.

	Number of cells			Radii		Volume		
	$N_{\alpha}$ (%)	$N_{\beta}$ (%)	Total (%)	$r_{\alpha}$ ( $\mu\text{m}$ ) n = 10879	$r_{\beta}$ ( $\mu\text{m}$ ) n = 27609	$\alpha$ -cells ( $\times 10^6 \mu\text{m}^3$ ) n = 10879	$\beta$ -cells ( $\times 10^6 \mu\text{m}^3$ ) n = 27609	Total ( $\times 10^6 \mu\text{m}^3$ ) n = 38488
Human	10879 (28.3)	27609 (71.7)	38488 (100)	Mean (SD) 4.8 (0.4)	Mean (SD) 5.3 (0.7)	2.5 (1.4)	Mean (SD) 9.3(5.1)	11.7 (6.5)
				Median (IQR) 4.7 (0.6)	Median (IQR) 5.1 (0.9)	2.5 (2.1)	Median (IQR) 9.3(9.5)	11.8(11.6)
Mouse	3637 (6.7)	50798 (93.3)	54435 (100)	Mean (SD) 5.2 (0.9)	Mean (SD) 5.2 (0.7)	1.2 (0.6)	Mean (IQR) 16.5 (10.6)	17.7 (11.3)
				Median (IQR) 4.9 (1.0)	Median (IQR) 5.0 (1.0)	1.0 (1.1)	Median (IQR) 14.5 (20.2)	15.6 (21.3)
Chi-square		7968 (df = 2)		U = 1.7E7	U = 6.6E8	t = 4.45 (df = 37.36)	t = 3.24 (df = 38.73)	t = 2.42 (df = 43.11)
P-value		<0.0001		<0.0001	<0.0001	P < .001	P < .01	P < .05

The percentages of  $\alpha$  and  $\beta$  cells differed between species. In human islets, 28.3% of islet cells were  $\alpha$  cells and 71.7% were  $\beta$  cells. In contrast, in mouse islets, only 6.7% were  $\alpha$  cells while 93.3% were  $\beta$  cells (see Table 2 and Figure 2(d)).

The median values of the radii of  $\alpha$  cells in the reconstructed human and mouse islets were  $\tilde{r}_{\alpha,h} = 4.74 \mu\text{m}$  and  $\tilde{r}_{\alpha,m} = 4.87 \mu\text{m}$ , respectively (Figure 2(e)). Similarly, the median radii of  $\beta$  cells were  $\tilde{r}_{\beta,h} = 5.09 \mu\text{m}$  and  $\tilde{r}_{\beta,m} = 4.97 \mu\text{m}$  in human and mouse islets, respectively (Figure 2(f)). It should be noted that, although statistically significant, the radii of  $\alpha$  and  $\beta$  cells in human and mouse islets (as well as the mean values presented in Table

2) were extremely similar, even though the experimentally derived distributions used in the reconstruction process were different. In terms of cell volumes, mouse islets had a higher average volume when compared to human islets (Figure 2(g)). The mean volume of  $\alpha$  cells was higher in human islets (Figure 2(h)). In contrast, mouse islets had a higher  $\beta$  cell volume than human islets (Figure 2(i)). These results suggest that volume differences between human and mouse islets are most likely due to the differences in the number of cells and not because of differences in cell size. Statistical details about the number, proportions, cell's radii and islet volumes can be consulted in Table 2.

**Table 3.** Cell-to-cell contact information obtained from the reconstruction process of human and mice islets

	Cell-to-cell contacts					
	$N_{\alpha\alpha}$ (%)	$N_{\alpha\beta}$ (%)	$N_{\beta\beta}$ (%)	Homotypic (%)	Heterotypic (%)	Total (%)
Human	10388 (18.2)	13733 (24.1)	32819 (57.6)	43207 (75.88)	13733 (24.12)	56940 (100)
Mouse	1228 (1.9)	5436 (8.6)	56672 (89.5)	57900 (91.42)	5436 (8.58)	63336 (100)
Chi-square (df = 1)		16880			5400	
P value		<0.0001			<0.0001	

$N_{\alpha\alpha}$ :  $\alpha$ - $\alpha$  contacts,  $N_{\beta\beta}$ :  $\beta$ - $\beta$  contacts,  $N_{\alpha\beta}$ :  $\alpha$ - $\beta$  contacts.

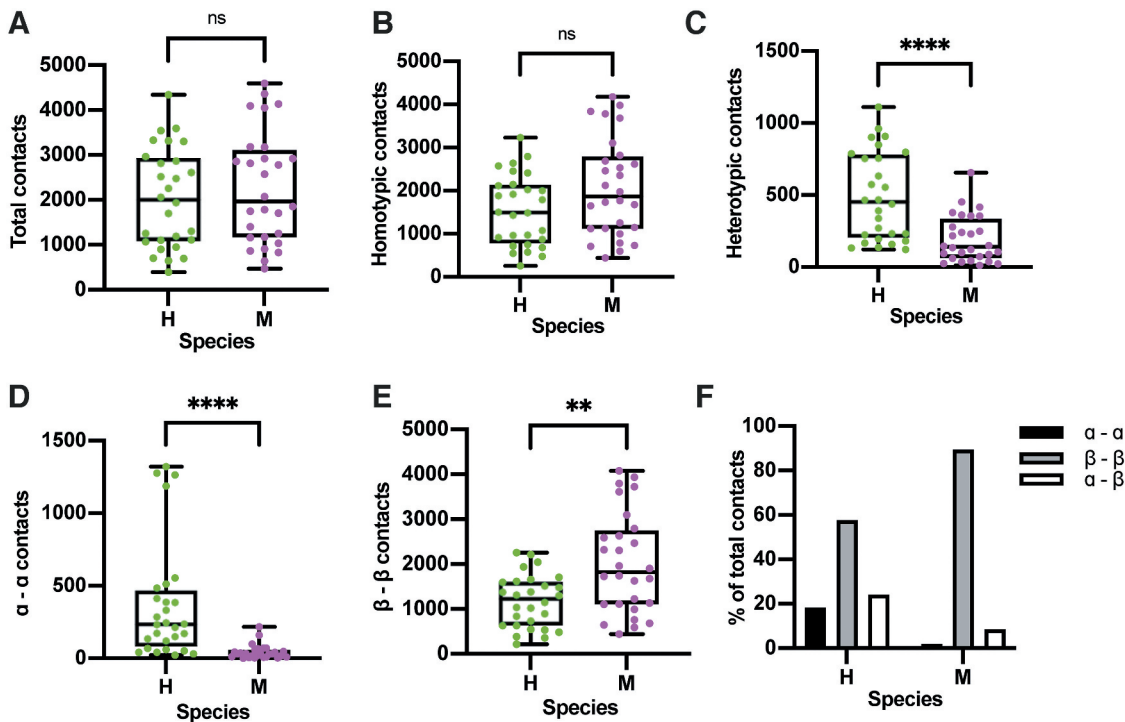


**Figure 3.** Cell-to-cell contacts in human and mice islets.

### Cell-to-cell contacts

As mentioned before, given that the analyzed islets were only composed of  $\alpha$  and  $\beta$  cells, only  $\alpha$ - $\alpha$ ,  $\beta$ - $\beta$  and  $\alpha$ - $\beta$  contacts were considered (Table 3). No differences in the average total number of cell-to-cell contacts were found between human and mouse islets (Figure 3(a)). Human islets had significantly more  $\alpha$ - $\alpha$  contacts than mouse islets (Figure 3(d)). In contrast, mouse islets had more  $\beta$ - $\beta$  contacts than human islets (Figure 3(e)). On the other hand, human islets had a higher number of  $\alpha$ - $\beta$  contacts in comparison to mouse islets (Figure 3(c)). Overall, as a percentage of total contacts, the percentages of  $\alpha$ - $\alpha$ ,  $\beta$ - $\beta$  and  $\alpha$ - $\beta$  contacts varied between human and mouse islets (Figure 3(f)). In human islets, 18.24% of total were  $\alpha$ - $\alpha$  contacts, 57.6%  $\beta$ - $\beta$  contacts and 24.1%  $\alpha$ - $\beta$  contacts. In contrast, in mouse islets only 1.9% were  $\alpha$ - $\alpha$  contacts, 89.5% were  $\beta$ - $\beta$  contacts and 8.6% were  $\alpha$ - $\beta$  contacts. As illustrated in Figures 3(b) and (c) (see also Table 3), the number of heterotypic contacts differed between species, being greater in human islets, while the number of homotypic contacts did not differ significantly. On the other hand, there were differences in the percentages of homotypic (i.e.  $\alpha$ - $\alpha$  and  $\beta$ - $\beta$ ) and heterotypic ( $\alpha$ - $\beta$ ) contacts between human and mouse islets, being homotypic 91.4% of contacts in mouse islets and 75.9% in human islets, while 8.6% and 24.1% were heterotypic, respectively

(see Table 3 and Figure 3(f)). According to our results, the great majority of homotypic contacts in mouse islets are  $\beta$ - $\beta$  contacts, which is reasonable if we consider that, as described above,  $\alpha$  cells only represent 6.7% of cells in the reconstructed mice islets. In contrast, in human islets both  $\alpha$ - $\alpha$  and  $\beta$ - $\beta$  contacts contributed considerably to the count of homotypic contacts, reflecting the much higher percentage of  $\alpha$  cells present in human islets.

### Structural networks

#### Networks of $\beta$ cells ( $\beta$ - $\beta$ )

As described in Table 4, where the network metrics are summarized, there were differences between human and mouse islets in both the average degree and clustering coefficient of the  $\beta$ - $\beta$  network (Figure 4(a and c)), although in both cases, the mean and median values were barely different (see Table 4). In contrast, there were not differences between species in the density, diameter and global efficiency of the  $\beta$ - $\beta$  network (Figure 4(b, d, e)). This results suggest that the connectivity between  $\beta$ -cells is marginally higher in mouse islets as a result of the higher proportion of  $\beta$ -cells and  $\beta$ - $\beta$  contacts (see Figures 2(c and e)). However, given the fact that the density, diameter and global efficiency was similar in both species, it is reasonable to conclude that networks of  $\beta$ -cells in mouse and human islets are similar from a topological viewpoint.

**Table 4.** Network metrics calculated from  $\beta$  -  $\beta$  and  $\alpha$  -  $\beta$  networks in human and mice islets.

Network	Degree		Density		Clustering		Diameter		Efficiency	
	$\beta$ - $\beta$	$\alpha$ - $\beta$	$\beta$ - $\beta$	$\alpha$ - $\beta$	$\beta$ - $\beta$	$\alpha$ - $\beta$	$\beta$ - $\beta$	$\alpha$ - $\beta$	$\beta$ - $\beta$	$\alpha$ - $\beta$
Human					Mean (SD)					
	1.7 (1.6)	3.0 (1.6)	1.7E-3 (1.2E-3)	2.8E-3 (1.6E-3)	0.08 (0.2)	0.1 (0.2)	49.1 (15.9)	34.3 (5.3)	0.03 (0.02)	0.08 (0.02)
					Median (IQR)					
	2.0 (3.0)	3.0 (2.0)	1.3E-3 (1.6E-3)	2.1E-3 (2.4E-3)	0.0 (1.0)	0.0 (0.2)	46.5 (17.5)	35.0 (7.75)	0.02 (0.03)	0.08 (0.02)
n	38488		28		38488		28			
Mouse					Mean (SD)					
	2.1 (1.5)	2.3 (1.5)	1.4E-3 (8E-4)	1.5E-3 (0.9E-3)	0.09 (0.2)	0.1 (0.2)	53.5 (20.5)	54.8 (20.2)	0.03 (0.03)	0.04 (0.03)
					Median (IQR)					
	2.0 (2.0)	2.0 (2.0)	1.3E-3 (9E-4)	1.3E-3 (1.3E-3)	0.0 (1.0)	0.0 (0.2)	53.0 (29.5)	57.0 (31.5)	0.02 (0.04)	0.03 (0.05)
n	54435		28		54435		28			
U	9E8	8E8	329	175	1E9	9E8	349	147.5	390	130
P-value	<0.0001	<0.0001	ns	<0.001	<0.0001	<0.0001	ns	<0.0001	ns	<0.0001

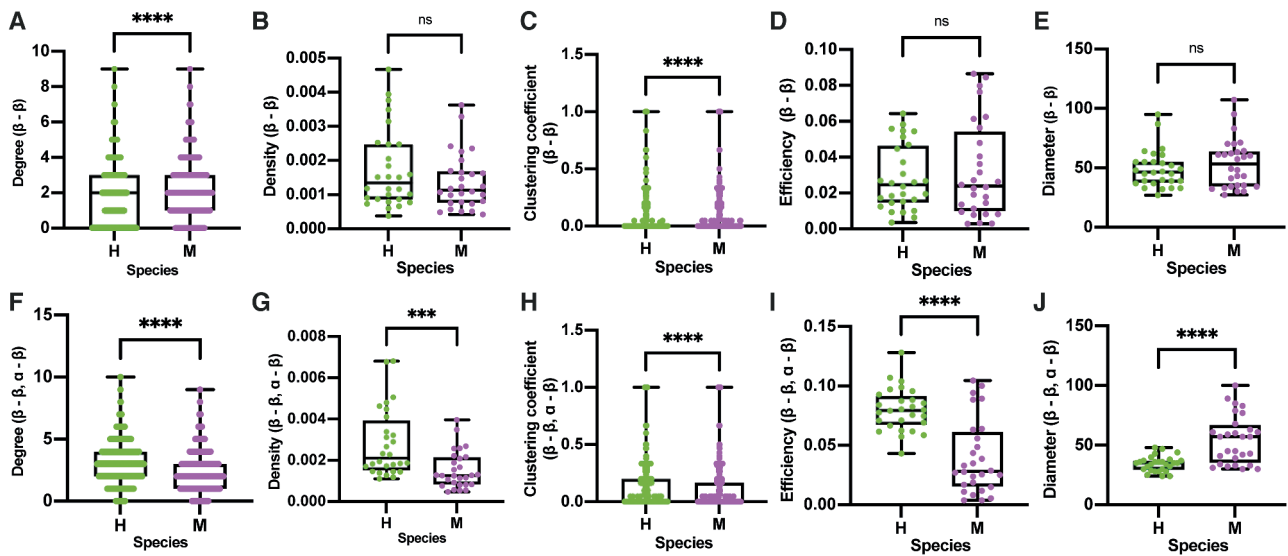


**Figure 4.** Figure 4. Network metrics calculated from the corresponding  $\beta$ - $\beta$  (A-E) and  $\alpha$ - $\beta$  (F-J) networks in mice and human islets.

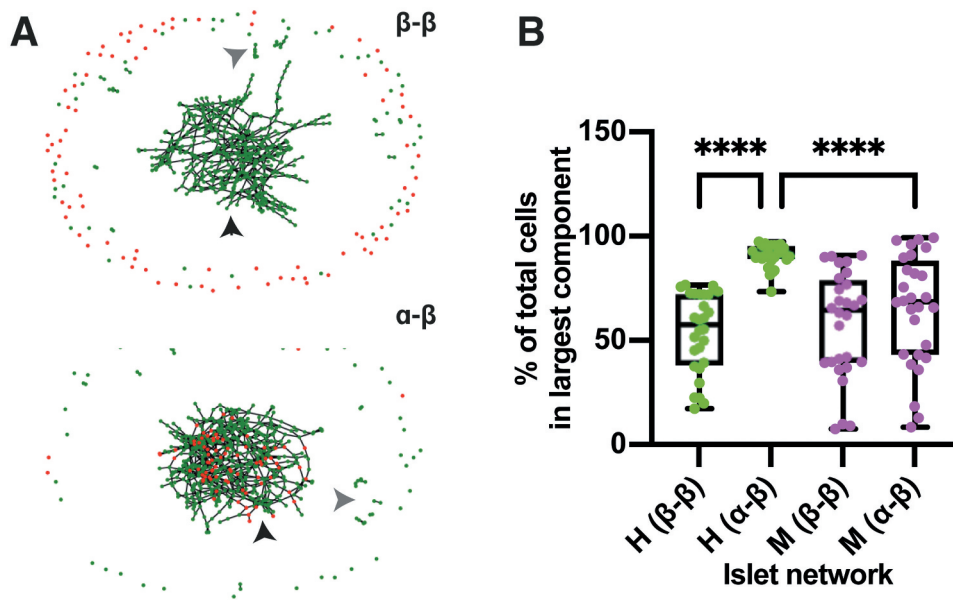


**Figure 5.** Components-02-02.tif.

### Networks of $\alpha$ and $\beta$ cells ( $\alpha$ - $\beta$ )

As also described in Table 4, when  $\alpha$  cells were added to the networks of  $\beta$  cells, both the average degree and density increased in both species as can be appreciated when Figure 4(a, b, f and g) are compared. It is worth noting that the  $\alpha$ - $\beta$  network of mouse islets showed a lower density when compared to that of human islets, which can be attributed to the fact that, on average, mouse islets had a higher number of cells, while the average number of total contacts between species showed no significant differences. On

the other hand, the average clustering coefficient showed only a slight increment in both species ( $\sim 25\%$  in humans and  $\sim 10\%$  in mice). Interestingly, the diameter of the networks in human islets decreased  $\sim 30\%$ , while in mice, on the contrary, the diameter increased slightly ( $\sim 10\%$ ). Moreover, the global efficiency of the  $\alpha$ - $\beta$  networks in human islets increased threefold, while in mice islets there was only a modest increase of 33%. These results indicate that the greater proportion of  $\alpha$  cells in human islets generates more efficient networks by increasing



the average number of connections in the network and reducing the path lengths between the network's nodes.

The islet networks were composed of several subnetworks or components disconnected from each other (see [Figure 5\(a\)](#)). As depicted in [Figure 5\(b\)](#), there were not differences between the percentage of cells in the largest component of  $\beta$ - $\beta$  networks from mice and human islets. Notably, when considering the  $\alpha$ - $\beta$  networks, the percentage of cells in the largest component increased considerably only in human islets ([Figure 5\(b\)](#)) while, according to our results, there were not differences between the largest components of the  $\beta$ - $\beta$  and  $\alpha$ - $\beta$  networks in mice islets. As shown in [Figure 5\(b\)](#), it is clear that the largest component in the  $\alpha$ - $\beta$  network in human islets is composed by a much larger percentage of cells than in mouse islets due to the considerable higher number of  $\alpha$ - $\beta$  contacts in human islets.

#### **Effects of the loss of $\beta$ -cells on cell-to-cell contacts and network metrics**

When 50% of  $\beta$ -cells was removed from the reconstructed islets (see the top panels of [Figure 6\(a\)](#) and (b)), the number of  $\beta$ - $\beta$  and  $\alpha$ - $\beta$  contacts, as well as the total contacts

decreased considerable in both species ([Figure 7\(a\)](#) and (b)). Specifically, the number of  $\beta$ - $\beta$  contacts dropped by  $\sim 75\%$  both in human and mouse islets. In contrast, the number of  $\alpha$ - $\beta$  contacts decreased  $\sim 50$  and  $19\%$  in mouse and human islets, respectively. Similarly, the total contacts decreased  $\sim 55$  and  $71\%$  in human and mouse islets, respectively.

The loss of  $\beta$ -cells, and as a consequence, of cell-to-cell contacts led to a corresponding decrease in all the network metrics (average degree, density, average clustering coefficient and global efficiency), as shown in [Figure 7\(c\)](#) and (d). In particular, the average degree dropped from  $3 \pm 1.6$  to  $1 \pm 1$  in human islets, and from  $2.3 \pm 1.5$  to  $0.7 \pm 0.8$  in mouse islets. Similarly, the density of the networks decreased from  $2.8E-3 \pm 1.6E-3$  to  $1.5E-3 \pm 0.9E-3$ , and from  $1.5E-3 \pm 0.9E-3$  to  $0.8E-3 \pm 0.5E-3$  in human and mouse islets, respectively. As expected, the global efficiency of the networks was severely affected, decreasing from  $0.08 \pm 0.02$  to  $3.8E-3 \pm 3E-3$  in human islets and from  $0.04 \pm 0.03$  to  $1.3E-3 \pm 0.9E-3$  in mouse islets. Likewise, the diameters were also affected, changing from  $34.3 \pm 6-3$  to  $17.71 \pm 10.57$  in human islets and from  $54.7 \pm 20.2$  to  $8 \pm 4.7$  in mouse islets. The impact of the loss  $\beta$ -cells can be clearly observed

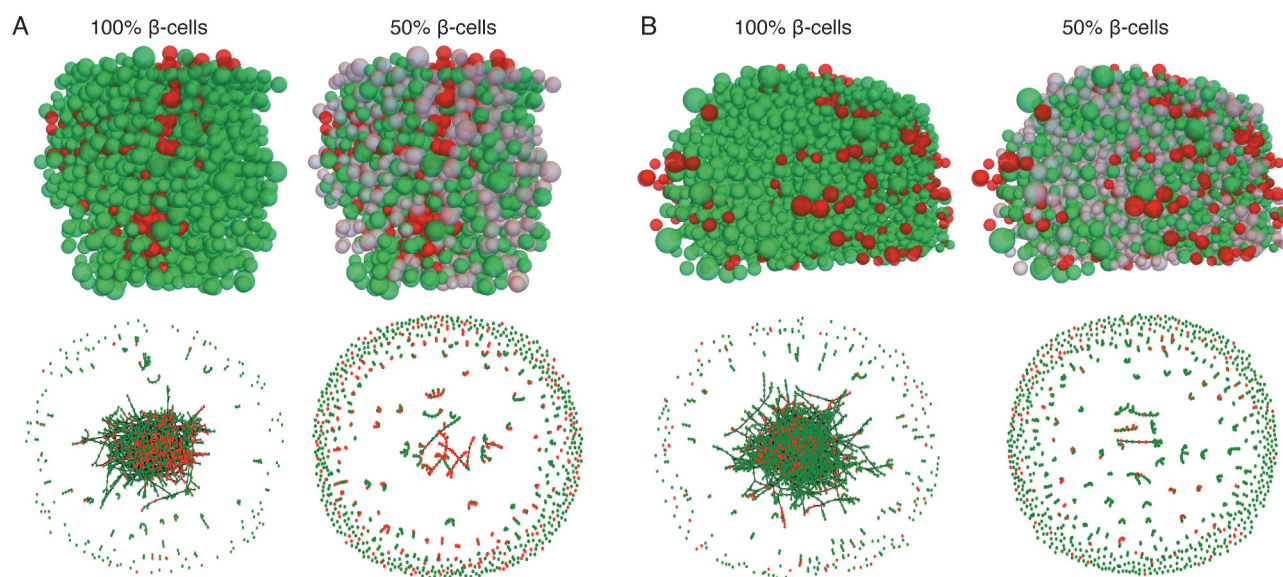


**Figure 6.** Example visualizations of the simulated loss of 50%  $\beta$ -cells in reconstructed human (A) and mouse (B) islets. The corresponding islet networks are shown below each islet.

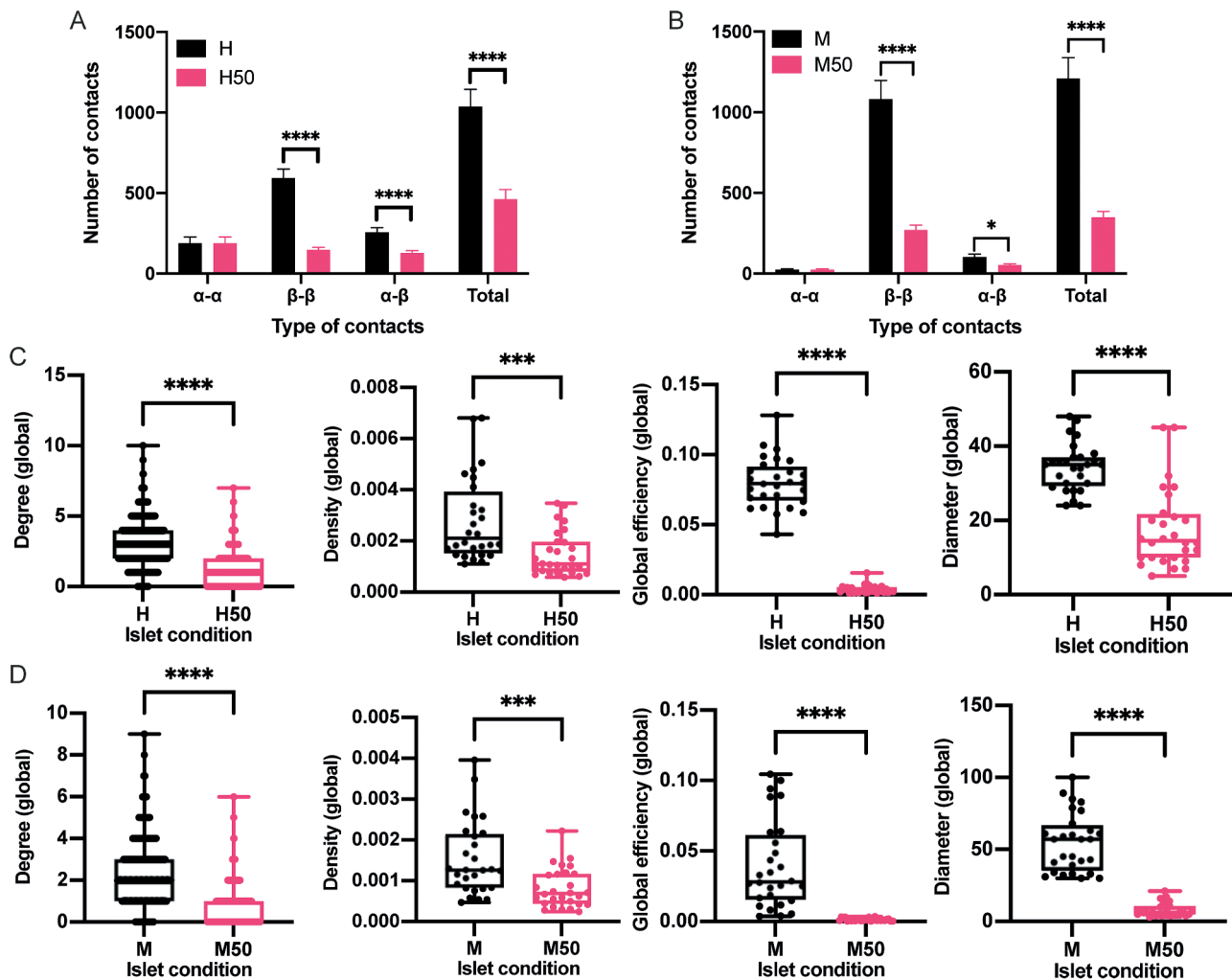


**Figure 7.** Effects of the loss of 50%  $\beta$ -cells in the cell-to-cell contacts and network metrics. A, B. Comparison of the number of cell-to-cell contacts in normal and perturbed islets (human and mice, respectively). C. Comparison of the network metrics between normal (H) and perturbed (H50) human islets. D. Comparison of the network metrics between normal (M) and perturbed (M50) mouse islets. Human and mouse islets with the loss of 50%  $\beta$ -cells are denoted as H50 and M50, respectively.

in the graphical representation of typical networks of normal and perturbed islets shown in the bottom panels of Figure 6(a) and (b).

## Discussion

In this article, we reconstructed human and mouse islets and performed a structural comparison using typical metrics such as volumes and proportion of cells, but also metrics obtained from the analysis of islet-derived networks.

We showed that the reconstruction algorithm used (for details see reference<sup>31</sup>) is capable of satisfactorily reconstructing islets from different species despite the differences in radii distributions and

proportions of cells. Notably, in most cases, the reconstructed islets included >99% experimentally identified cells.

According to our results, mouse islets are generally larger than human islets in terms of both the number of cells (as previously described by Hoang et al.<sup>22</sup>) and cell volume. In addition, the proportion of  $\alpha$  and  $\beta$  cells differed considerably between the two species, being the proportion of  $\beta$  cells larger in mouse islets and the proportion of  $\alpha$  cells larger in human islets, as it has been previously reported.<sup>14,19–24</sup> Interestingly, despite the differences in islet size, the number of total cell-to-cell contacts was not statistically different, although there were in fact important differences in the

proportion of  $\alpha$ - $\alpha$ ,  $\beta$ - $\beta$  and  $\alpha$ - $\beta$  contacts. Particularly, it is worth highlighting that  $\beta$ - $\beta$  contacts are considerably higher in mouse islets while in human islets there was a much greater proportion of  $\alpha$ - $\beta$  and  $\alpha$ - $\alpha$  contacts. As a result, from the analysis of the resulting islet networks, we found that the organization of  $\alpha$  and  $\beta$  cells in human islets constitutes a more efficient network from a connectivity viewpoint since there was a three-fold increase in the global efficiency of the  $\alpha$ - $\beta$  network in human islets when compared to the corresponding  $\beta$ - $\beta$  network, while the global efficiency of the  $\alpha$ - $\beta$  network in mouse islets increased only marginally in comparison to the  $\beta$ - $\beta$  network formed in mouse islets

Experimentally, functional networks have been constructed based on the correlations of  $\text{Ca}^{2+}$  signals measured in mouse islets.<sup>36–40</sup> In such studies, it has been shown that metrics estimated from functional networks evolve depending on the stimulatory regimen (low glucose before stimulation, activation, high glucose, deactivation and low glucose after stimulation), being the average degree, the global efficiency and the average clustering coefficient metrics that increase as a response of glucose stimulation.<sup>36</sup> Similarly, Markovic et al.<sup>37</sup> and Salem et al.<sup>39</sup> showed that the connectivity of networks of  $\beta$  cells increases as the stimulatory glucose level increases, as indicated by the change in the value of network metrics calculated. In addition, their results also suggest that the network of  $\beta$  cells becomes more integrated as the levels of glucose are increased by recruiting subnetworks that are segregated at lower or non-stimulatory levels. Other studies,<sup>39,40</sup> based on the analysis of islet networks, have described the presence of hubs composed of ~1-10% of  $\beta$ -cells that, according to the authors, serve as pacemakers for the islet response to a glucose stimulus. On the other hand, in a recent work, Stozar et al.<sup>38</sup> showed that the fast oscillatory behavior of  $\beta$  seems to be locally clustered, while slow oscillations were associated to long-range and global connections. In the light of the inter-species differences reported in this article, all these experimental results must be evaluated

and corroborated in human islets in order to determine the functional implications of the structural differences between species.

While it is still difficult to determine a definitive relationship between the network metrics and the functional properties of the islets, it is reasonable to hypothesize that the network metrics could serve as indicators of the islet capability to exhibit an organized response, as they provide us with a quantitative measure of local (e.g. degree, clustering coefficient) and global properties (e.g. density, global efficiency and diameter) of the islet connectivity network. For instance, a decrease in the average degree as a consequence of the loss of  $\beta$ -cells could be indicating that regulatory inputs from neighbor cells might be missing as a result, and therefore local coordination and/or regulation could be impaired. Similarly, a decrease in the density, diameter and global efficiency of the islet network could indicate that the transmission of stimulatory and/or inhibitory signals from one islet region to another could be also impaired as a consequence of a reduced inra-islet connectivity.

In this work, we have used network analysis to characterize the structural networks in mouse and human islets, and therefore, functional aspects were not explicitly considered. In spite of this, we believe that the use of network-derived metrics in conjunction with morphological indicators will contribute to elucidate the relationship between the structural and functional properties of pancreatic islets, and eventually, to contribute to gain a better understanding of islet dysfunction in pathological conditions such as type 1 or 2 diabetes.

## Acknowledgments

G. J. Félix-Martínez thanks CONACYT (National Council of Science and Technology, México), the Department of Electrical Engineering and the Laboratorio Nacional de Cómputo de Alto Desempeño (LANCAD) of the Universidad Autónoma Metropolitana, Unidad Iztapalapa, México, for the support given to this work. Once again, we thank Dr. Danh-Tai Hoang, Dr. Manami Hara and Dr. Junghyo Jo for their generosity in sharing the islet architecture data with the research community.

## Disclosure statement

No potential conflict of interest was reported by the author(s).

## ORCID

Gerardo J. Félix-Martínez  <http://orcid.org/0000-0001-8901-4836>

## References

- Noguchi GM, Huising MO. Integrating the inputs that shape pancreatic islet hormone release. *Nat Metab.* 2019;1(12):1189–1201. PMID: 32694675. doi:10.1038/s42255-019-0148-2
- Moreno AP, Berthoud VM, Pérez-Palacios G, Pérez-Armendariz EM. Biophysical evidence that connexin-36 forms functional gap junction channels between pancreatic mouse  $\beta$ -cells. *Am J Physiol Endocrinol Metab.* 2005;288(5):E948–56. PMID: 15625088. doi:10.1152/ajpendo.00216.2004
- Pérez-Armendariz EM. Connexin 36, a key element in pancreatic beta cell function. *Neuropharmacology.* 2013;75:557–566. PMID: 23973309. doi:10.1016/j.neuropharm.2013.08.015.
- Speier S, Gjinovci A, Charollais A, Meda P, Rupnik M. Cx36-mediated coupling reduces  $\beta$ -cell heterogeneity, confines the stimulating glucose concentration range, and affects insulin release kinetics. *Diabetes.* 2007;56:1078–1086. PMID: 17395748. doi:10.2337/db06-0232.
- Serre-Beinier V, Bosco D, Zulianello L, Charollais A, Caille D, Charpentier E, Gauthier BR, Diaferia GR, Giepmans BN, Lupi R, et al. Cx36 makes channels coupling human pancreatic  $\beta$ -cells, and correlates with insulin expression. *Hum Mol Genet.* 2009;18(3):428–439. PMID: 19000992. doi:10.1093/hmg/ddn370.
- Düfer M. Gap junctional communication between  $\beta$ - and  $\delta$ -cells: another player for suppression of glucagon release. *J Physiol.* 2018;596(2):131–132. PMID: 29193084. doi:10.1113/JP275329
- Briant LJB, Reinbothe TM, Spiliotis I, Miranda C, Rodriguez B, Rorsman P.  $\delta$ - and  $\beta$ -cells are electrically coupled and regulate  $\alpha$ -cell activity via somatostatin. *J Physiol.* 2017;17:3281. PMID: 28975620. doi:10.1113/JP274581.
- Caicedo A. Paracrine and autocrine interactions in the human islet: more than meets the eye. *Semin Cell Dev Biol.* 2013;24(1):11–21. PMID: 23022232. doi:10.1016/j.semcdb.2012.09.007
- Koh D-S, Cho J-H, Chen L. Paracrine interactions within islets of Langerhans. *J Mol Neurosci.* 2012;48(2):429–440. PMID: 22528452. doi:10.1007/s12031-012-9752-2
- Henquin J-C. Paracrine and autocrine control of insulin secretion in human islets: evidence and pending questions. *Am J Physiol Endocrinol Metab.* 2021;320(1):E78–86. PMID: 33103455. doi:10.1152/ajpendo.00485.2020
- Rodriguez-Diaz R, Tamayo A, Hara M, Caicedo A. The local paracrine actions of the pancreatic  $\alpha$ -cell. *Diabetes.* 2020;69(4):550–558. PMID: 31882565. doi:10.2337/dbi19-0002
- Arrojo e Drigo R, Ali Y, Diez J, Srinivasan DK, Berggren P-O, Boehm BO. New insights into the architecture of the islet of Langerhans: a focused cross-species assessment. *Diabetologia.* 2015;58(10):2218–2228. PMID: 26215305. doi:10.1007/s00125-015-3699-0
- Roscioni SS, Migliorini A, Gegg M, Lickert H. Impact of islet architecture on  $\beta$ -cell heterogeneity, plasticity and function. *Nat Rev Endocrinol.* 2016;1–15. 27585958. doi:10.1038/nrendo.2016.147.
- Cabrera O, Berman DM, Kenyon NS, Ricordi C, Berggren P-O, Caicedo A. The unique cytoarchitecture of human pancreatic islets has implications for islet cell function. *Proc Natl Acad Sci U S A.* 2006;103(7):2334–2339. PMID: 16461897. doi:10.1073/pnas.0510790103
- Folli F, La Rosa S, Finzi G, Davalli AM, Galli A, Dick EJ, Perego C, Mendoza RG. Pancreatic islet of Langerhans' cytoarchitecture and ultrastructure in normal glucose tolerance and in type 2 diabetes mellitus. *Diabetes Obes Metab.* 2018;20:137–144. PMID: 30230173. doi:10.1111/dom.13380.
- Westermarck P, Andersson A, Westermarck GT. Islet amyloid polypeptide, islet amyloid, and diabetes mellitus. *Physiol Rev.* 2011;91(3):795–826. doi:10.1152/physrev.00042.2009.
- Kilimnik G, Zhao B, Jo J, Periwal V, Witkowski P, Misawa R, Hara M. Altered islet composition and disproportionate loss of large islets in patients with type 2 diabetes. *Plos One.* 2011;6:e27445. PMID: 22102895. doi:10.1371/journal.pone.0027445.
- Bosco D, Armanet M, Morel P, Niclauss N, Sgroi A, Muller YD, Giovannoni L, Parnaud G, Berney T. Unique arrangement of alpha- and beta-cells in human islets of Langerhans. *Diabetes.* 2010;59:1202–1210. PMID: 20185817. doi:10.2337/db09-1177.
- Kilimnik G, Jo J, Periwal V, Zielinski MC, Hara M. Quantification of islet size and architecture. *Islets.* 2012;4(2):167–172. PMID: 22653677. doi:10.4161/isl.19256
- Brissova M, Fowler MJ, Nicholson WE, Chu A, Hirshberg B, Harlan DM, Powers AC. Assessment of human pancreatic islet architecture and composition by laser scanning confocal microscopy. *J Histochem Cytochem.* 2005;53(9):1087–1097. PMID: 15923354. doi:10.1369/jhc.5C6684.2005
- Kim A, Miller K, Jo J, Kilimnik G, Wojcik P, Hara M. Islet architecture: a comparative study. *Islets.* 2009;1(2):129–136. PMID: 20606719. doi:10.4161/isl.1.2.9480

22. Hoang D-T, Matsunari H, Nagaya M, Nagashima H, Millis JM, Witkowski P, Perival V, Hara M, Jo J. A conserved rule for pancreatic islet organization. *Plos One*. 2014;9:e110384. PMID: 25350558. doi:10.1371/journal.pone.0110384.
23. Ionescu-Tirgoviste C, Gagniuic PA, Gubceac E, Mardare L, Popescu I, Dima S, Militaru M. A 3D map of the islet routes throughout the healthy human pancreas. *Sci Rep*. 2015;5(1):1–14. PMID: 26417671. doi:10.1038/srep14634
24. Wiczorek G, Pospischil A, Perentes E. A comparative immunohistochemical study of pancreatic islets in laboratory animals (rats, dogs, minipigs, nonhuman primates). *Exp Toxicol Pathol*. 1998;50(3):151–172. PMID: 9681646. doi:10.1016/S0940-2993(98)80078-X
25. Rorsman P, Ashcroft FM. Pancreatic  $\beta$ -cell electrical activity and insulin secretion: of mice and men. *Physiol Rev*. 2018;98(1):117–214. PMID: 29212789. doi:10.1152/physrev.00008.2017
26. Félix-Martínez GJ, Godínez-Fernández JR. Mathematical models of electrical activity of the pancreatic  $\beta$ -cell: a physiological review. *Islets*. 2014;6(3):e949195. PMID: 25322829. doi:10.4161/19382014.2014.949195
27. Harrison DE, Christie MR. Properties of isolated human islets of Langerhans: insulin secretion, glucose oxidation and protein phosphorylation. *Diabetologia*. 1985;28(2):99–103. PMID: 3884420. doi:10.1007/BF00279924
28. Henquin JC, Dufrane D, Nenquin M. Nutrient control of insulin secretion in isolated normal human islets. *Diabetes*. 2006;55(12):3470–3477. PMID: 17130494. doi:10.2337/db06-0868
29. Rorsman P, Braun M. Regulation of insulin secretion in human pancreatic islets. *Annu Rev Physiol*. 2013;75(1):155–179. PMID: 22974438. doi:10.1146/annurev-physiol-030212-183754
30. Drews G, Krippeit-Drews P, Düfer M. Electrophysiology of islet cells. *Adv Exp Med Biol*. 2010;654:115–163. PMID: 20217497. doi:10.1007/978-90-481-3271-3\_7.
31. Félix-Martínez GJ, Mata A, Godínez-Fernández JR. Reconstructing human pancreatic islet architectures using computational optimization. *Islets*. 2020;12(6):121–133. PMID: 33090076. doi:10.1080/19382014.2020.1823178
32. Hoang D-T, Hara M, Jo J. Design principles of pancreatic islets: glucose-dependent coordination of hormone pulses. *PloS One*. 2016;11:e0152446. PMID: 27035570. doi:10.1371/journal.pone.0152446.
33. Camunas-Soler J, Dai X-Q, Hang Y, Bautista A, Lyon J, Suzuki K, Kim SK, Quake SR, MacDonald PE. Patch-seq links single-cell transcriptomes to human islet dysfunction in diabetes. *Cell Metab*. 2020;31(5):1017–1031.e4. PMID: 32302527. doi:10.1016/j.cmet.2020.04.005
34. Briant LJB, Zhang Q, Vergari E, Kellard JA, Rodriguez B, Ashcroft FM, Rorsman P. Functional identification of islet cell types by electrophysiological fingerprinting. *J R Soc Interface*. 2017;14(128):20160999. PMID: 28275121. doi:10.1098/rsif.2016.0999
35. Hagberg AA, Schult DA, Swart PJ Exploring network structure, dynamics, and function using networkX, in Proceedings of the 7th Python in Science Conference (SciPy2008). Varoquaux G, Vaught T, Millman J (Eds), (Pasadena, CA USA), pp. 11–15, Aug 2008.
36. Stožer A, Gosak M, Dolenšek J, Perc M, Marhl M, Rupnik MS, Korošak D. Functional connectivity in islets of langerhans from mouse pancreas tissue slices. *Plos Comp Biol*. 2013;9:e1002923. PMID: 23468610. doi:10.1371/journal.pcbi.1002923.
37. Markovič R, Stožer A, Gosak M, Dolenšek J, Marhl M, Rupnik MS. Progressive glucose stimulation of islet beta cells reveals a transition from segregated to integrated modular functional connectivity patterns. *Sci Rep*. 2015;5(1):1–10. PMID: 25598507. doi:10.1038/srep07845
38. Stožer A, Gosak M. Assessing different temporal scales of calcium dynamics in networks of beta cell populations. *Front Physiol*. 2021;12(16). PMID: 33833686. doi:10.3389/fphys.2021.612233
39. Salem V, Silva LD, Suba K, Georgiadou E, Ne Da Mousavy Gharavy S, Akhtar N, Martin-Alonso A, Gaboriau DCA, Rothery SM, Stylianides T, et al. Leader  $\beta$ -cells coordinate Ca<sup>2+</sup> dynamics across pancreatic islets in vivo. *Nat Metab*. 2019;1(6):615–629. PMID: 32694805. doi:10.1038/s42255-019-0075-2.
40. Johnston NR, Mitchell RK, Haythorne E, Pessoa MP, Semplici F, Ferrer J, Piemonti L, Marchetti P, Bugliani M, Bosco D, et al. Beta cell hubs dictate pancreatic islet responses to glucose. *Cell Metab*. 2016;24(3):389–401. PMID: 2745214. doi:10.1016/j.cmet.2016.06.020.